Lasers in Manufacturing Conference 2025

Experimental Investigation of Shielding and Carrier Gases in Laser Material Deposition: Impact on Microstructure, Hardness, and Cost Efficiency

E. Weisser[a,*], P. Kiefer[a], V. Glushych[a], R. Hama-Saleh Abdullah[a]

[a]*Fraunhofer Institute for Laser Technology (ILT), Steinbachstrasse 15, 52076 Aachen, Germany*

Abstract

This study investigates the influence of process gases on the laser material deposition process, with a particular focus on their effects on geometric characteristics of single tracks, process temperature and microhardness. The research aims to analyze the interactions between the selected process gases argon, helium, nitrogen, and carbon dioxide and the powder material 316L. A comparative evaluation with laser welding techniques highlights shared principles and distinct effects, providing a comprehensive understanding of process dynamics. Experimental investigations and literature analyses reveal the critical impact of gas flow rates, chemical reactivity, and thermal conductivity on the resulting layer quality and structural properties. The findings contribute to optimizing process parameters, ensuring enhanced material performance and reliability in industrial applications. This work serves as a foundation for future studies on tailored gas applications in laser-based manufacturing processes.

Keywords: Laser Material Deposition; Process Gases; 316L; Argon; Helium; Nitrogen; Carbon Dioxide; Microstructure; Dilution Zone; Heat-Affected Zone; Microhardness; Process Temperature

1. Introduction

In additive manufacturing, the choice of process gas is crucial for determining the quality and properties of the final product (Ahn et al. 2017). Process gases, i.e. shielding and carrier gases, influence microstructure, mechanical performance, melt pool dynamics, and surface characteristics (Bliedtner et al. 2013). Additionally, they affect heat distribution, either by enhancing heat dissipation or promoting exothermic reactions (Ruiz et al. 2018; Wank et al. 2018). They also play a key role in terms of porosity (Wank et al. 2018; Elmer et al. 2014). From an economic standpoint, process gas is a major cost driver in laser metal deposition (LMD), alongside energy and material costs. Long processing times and low deposition rates increase gas consumption, often making gas more expensive than the metal powder itself (Witzel 2014; Härtl und Zäh 2002). Therefore, optimizing process gas selection can significantly reduce overall costs, as shown in Table 1.

Table 1: Process gas operating costs in €/h (Linde Gas 2025)

	argon	helium	nitrogen	carbon dioxide
[€/h]	17,20	67,71	12,70	21,61

* Corresponding author, Eduard Weisser M.Sc., Tel.: +49 241 8906 442;
E-mail address: eduard.weisser@ilt.fraunhofer.de.

Prior to this work, only a limited number of studies systematically investigated the influence of different process gases on the LMD process. In contrast, the use of argon as process gas is widespread for LMD (Dobbelstein et al. 2019; Candel-Ruiz et al. 2015; Zhao et al. 2024). To categorize the effects of various process gases, studies on LMD but also investigations of related processes – such as laser beam welding and laser cladding – are also considered due to their procedural similarities., (Bliedtner et al. 2013; Ruiz et al. 2018)

In LMD, a distinction must be made between the shielding gas flow rate, which primarily protects the laser optics and accounts for the majority of melt pool coverage, and the carrier gas flow rate, which mainly serves as a transport medium for powder particles into the process (Bliedtner et al. 2013). Several previous studies have analyzed process gases regarding their effectiveness in shielding the melt pool via the locally formed protective gas atmosphere and the resulting residual oxygen content (Zhang et al. 2023; Kaljevic und Demir 2022). Zhang et al. investigated the effects of increased oxygen content on the processability of Ti6Al4V and demonstrated that changes in microstructural composition occur when the oxygen content exceeds 1000 ppm. An increase in residual oxygen content may result from insufficient melt pool coverage quality. Furthermore, the use of reactive oxidizing process gases such as carbon dioxide can influence both the surface tension of the molten material and the flow behavior within the melt pool due to the formation of oxide layers (Leimser 2008; Härtl und Zäh 2002; Schulze G. 2010). For a nickel-based self-fluxing alloy, Wank et al. observed an increased emission intensity in the melt pool when employing carbon dioxide as process gas. The elevated temperature in the melt pool is associated with reduced hardness values using carbon dioxide as process gas. Simultaneously, dendritic grain structures were identified in the microstructure when using carbon dioxide. Ruiz et al. reported an increasing melt pool temperature for Inconel 718 when helium was added to the process gas mixture.

While the aforementioned studies have examined individual gases and their specific effects on the process, such as melt pool shielding, thermal conductivity, or resulting microstructure and hardness, this study aims to provide a comprehensive overview of different process gases for a single material, based on both single-track and volumetric builds.

2. Experimental Setup and Procedure

The experimental setup includes a Trumpf TruDisk 4006 laser source. It delivers up to 4000 W of laser power at a wavelength of λ = 1030 nm and is coupled to the system via fiber optics. The laser forms a Gaussian intensity profile with a beam diameter of 1.5 mm. The focusing optics (Trumpf BEO70) and powder nozzle (HighNo 4.0, HD Sonderoptiken GmbH & Co. KG) are mounted on a CNC-controlled 3-axis system (Bosch Rexroth AG). Powder material is delivered by a powder feeder (GTV Verschleißschutz GmbH) via a rotating disk and carrier gas into the nozzle, where it is focused to a 9 mm stand-off through an annular gap. Shielding gas is supplied separately through the central nozzle channel, co-axially with the laser beam. Gas flow rates of shielding and carrier gas are monitored by two flow meters (Kobold Messring GmbH) and controlled via float-type flow regulators. In the experimental series, the process gases argon, helium, nitrogen, and carbon dioxide were systematically varied. For each test series, both the shielding gas and the carrier gas were simultaneously adjusted to the same gas type.

For the experimental series, the austenitic stainless- steel powder 316L (F-316LX-BR2, LSN Diffusion Ltd.) was used. The powder was produced by gas atomization and had a particle size range of 20–53 µm. S235 steel plates (100 × 100 × 10 mm) served as substrates. Prior to processing, their surfaces were milled and sandblasted. For the experiments, a previously developed LMD parameter set was used, which is presented in Table 2, to achieve a suitable aspect ratio for subsequent volume build-up.

Table 2. Parameter set for a laser spot diameter of 1.5 mm

laser power	feed rate	powder mass flow	shielding gas flow	carrier gas flow
1200 W	1000 mm/min	3.4 g/min	10 l /min	3 l/min

For single track analysis, a 30 mm long track is deposited twice to reduce measurement uncertainty and increase the statistical significance with a 10 mm spacing and evaluated using three cross-sections each. To study the influence of process gases on volumetric build-up, two cubic volumes (15 mm edge length) are produced per process gas. A total of 20 layers are deposited, with a 3-minute cooling break after 10 layers. Since the geometry of single tracks varies with the process gas, the track offset is adjusted to maintain a constant relative overlap of ~50 % of the track width. Similarly, the layer height offset in z-direction is adapted to achieve a relative overlap of ~120 % of the track height.

3. Evaluation Methodology

To comprehensively evaluate the geometrical, thermal, and microstructural characteristics resulting from the deposition process, a series of analytical and imaging techniques were applied. The following section outlines the preparation steps and measurement procedures used to assess single tracks and built-up volumes. Optical profilometry (Keyence VR5000) was used to determine track width and height of the single tracks, with 50 transverse profiles extracted per track to compute average geometry. The samples were sectioned and hot-embedded in phenolic resin, then ground and polished using diamond suspension up to 1 µm. Statistical significance was ensured by preparing three cross-sections from different positions along each single track and two from each of the built volumes. To visualize the heat-affected zone (HAZ) and distinguish the substrate from the deposited tracks, the cross-sections were etched using a 3% nitric acid solution, which selectively attacks the substrate material. To reveal the microstructure, the samples were additionally electrolytically etched in 10% oxalic acid for the single tracks, and a nitric hydrofluoric acid-based V2A etching solution for the built volumes. Light microscopic images of all cross-sections were acquired at 300× magnification using a Keyence VHX-6000 digital microscope. Using the images, dilution depth and HAZ depth were measured. Microhardness testing was performed using a QATM Qness (ATM Qness GmbH Qness 30 A+) hardness tester and the Vickers indentation method with a load of HV0.1 for the built volumes with approx. 300 indents distributed across a 15 × 10 mm area with a 1 mm horizontal and a one-layer height vertical spacing. The thermal process signature was captured using infrared thermography (InfraTec ImageIR 7350). Maximum temperatures were recorded using a filtered range of 700–2100 °C and averaged along a 127-pixel line. An emissivity of 0.45 was assumed for all analyses (Auer 2005). The maximum temperatures are accumulated along a fixed line spanning 127 pixels across the center of the single tracks for all sequences. The resulting mean value and standard deviation of the accumulated temperature data are then calculated and reported.

4. Results and Discussions

4.1. Influence of the process gases on the geometric characteristics of single tracks

Figure 1 shows the track width and track height of the single tracks for the different process gases argon, helium, nitrogen, and carbon dioxide for the powder material 316L. The single track width is not significantly varying when using argon, helium, or nitrogen as process gas. In contrast, the use of carbon dioxide gas leads to an increase in track width of approximately 200 µm. Notably, the track width under argon, helium, and nitrogen remains below the laser beam diameter of 1.5mm, while under carbon dioxide gas, a wider melt pool is formed. Regarding track height, an increase of approximately 30 µm is observed under nitrogen and about 40 µm under carbon dioxide, compared to the track heights achieved using argon and helium. This indicates a greater material accumulation when employing these reactive gases.

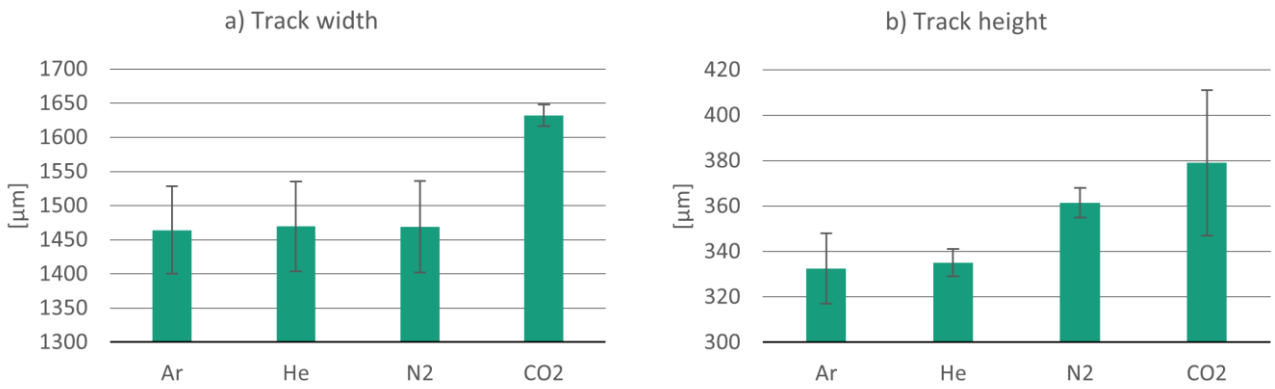

Fig. 1. (a) Width and (b) Height of single tracks deposited with different process gases using an identical process parameter set

4.2. Analysis of cross-sections of single t racks and built-up volumes

A comparison of the cross-sections of the single tracks, as displayed in Figure 2, reveals that the geometry of the material deposited using carbon dioxide gas deviates significantly from that produced with the other process gases. Using carbon dioxide gas, the dilution zone is reduced and the wetting angle decreases, while the track width increases and the height decreases, as previously shown by the optical profilometry results. The microstructure of the deposited material is similar for argon and helium, exhibiting relatively fine grain structures. In contrast, nitrogen results in greater variation in grain orientation and size, with some grains oriented perpendicular to the solidification direction. In the case of carbon dioxide gas, even larger grains are observed, predominantly oriented toward the center of the deposited contour.

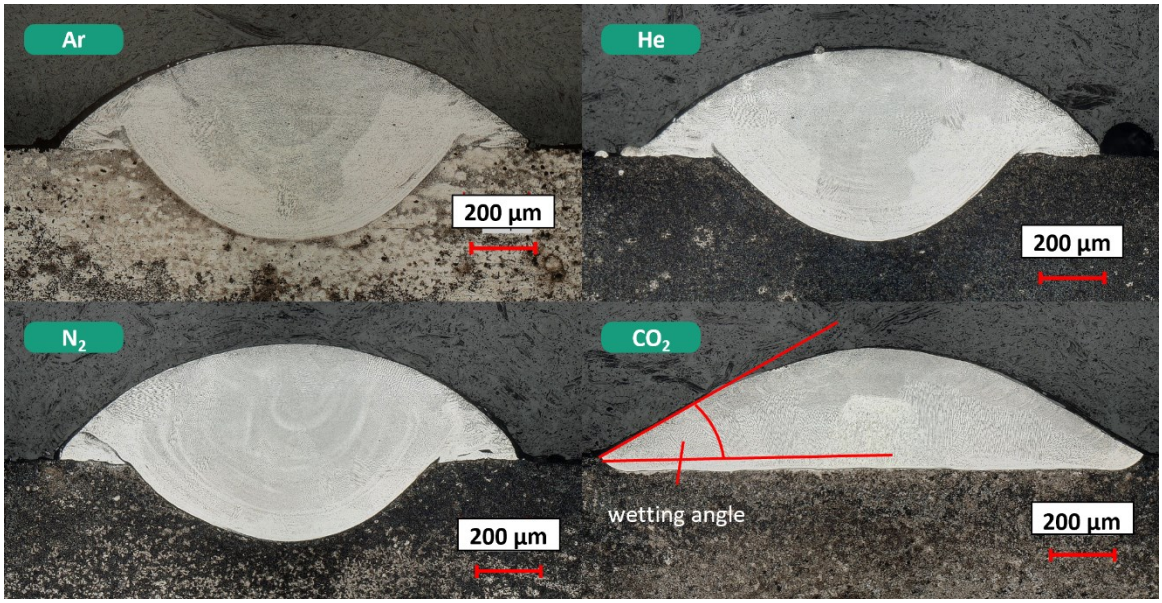

Fig. 2 Etched cross-sections of single tracks deposited using different process gases

Figure 3 presents the depth of the dilution zone and the HAZ for single tracks produced with different process gases using the investigated powder material. A significant reduction in the dilution depth of approximately 250 µm is observed when using carbon dioxide, compared to argon and helium. In contrast, nitrogen results in a slight reduction of about 30 µm. With respect to the HAZ, the shielding gases argon, helium, and nitrogen show negligible influence on its depth, whereas carbon dioxide leads to a reduction of approximately 100 µm. The results suggest that carbon dioxide as a process gas influences the surface tension of the melt pool, leading to generally wider single tracks with a reduced dilution zone. While no clear conclusions regarding melt pool flow can be drawn from the cross-sections, a reduction or suppression of melt pool dynamics is assumed, consistent with findings reported in (Leimser 2008; Czerner 2005).

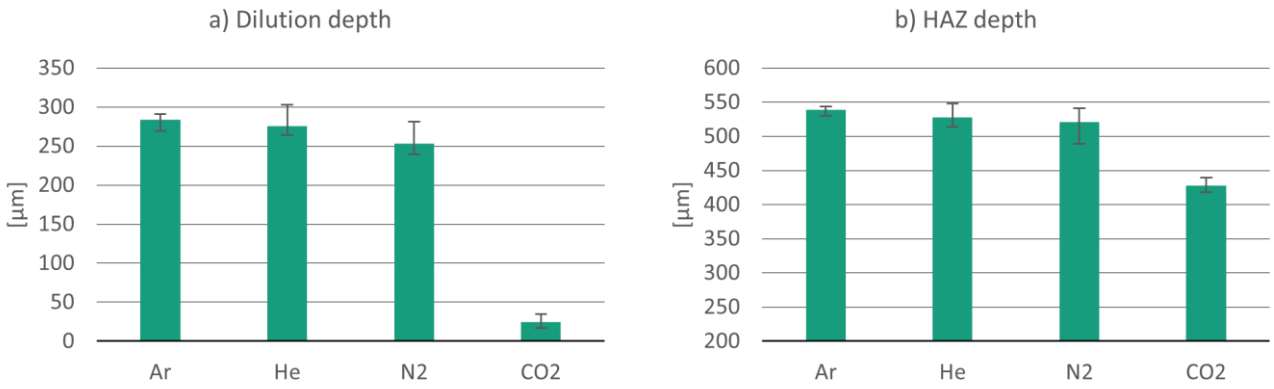

Fig. 3. (a) Depth of dilution zone and (b) depth of HAZ for the single tracks for different process gases

Figure 4 shows cross-sections of the built-up volumes of the investigated powder material processed with different process gases. A slight contour bulge at the edges is observed when using argon, which becomes more pronounced with helium and nitrogen, and is most prominent with carbon dioxide. When using carbon dioxide, the lateral layer build-up occurs nearly perpendicular to the substrate surface. Furthermore, the number of adhering powder particles on the sides of the volumes is significantly reduced with carbon dioxide. Cross-sections of the volumes built under argon, helium, and nitrogen reveal a uniform geometric arrangement of the offset single tracks. Under nitrogen, coarser grain structures spanning several layers are observed, whereas finer grains dominate with argon and helium. Using carbon dioxide gas, the individual layers and tracks exhibit increased width, resulting in greater overlap. In the center of the volume processed with carbon dioxide, large grain structures are observed that extend across multiple layers. Toward the edges, the microstructure becomes finer. Additionally, defects are found in the upper region of the carbon dioxide-processed volumes.

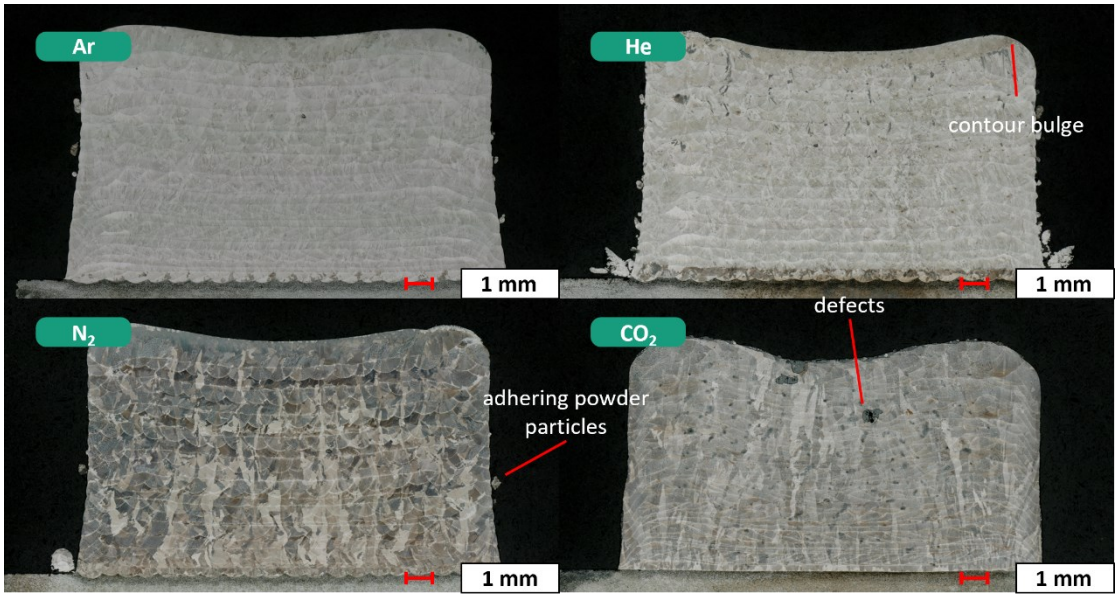

Fig. 4. Etched cross-sections of the built-up volumes for different process gases

Figure 5 presents the depth of the dilution zone and HAZ for the built-up volumes of the investigated powder material processed with different shielding gases. Compared to argon, the dilution depth increases by approximately 50 µm when using helium and by about 30 µm with nitrogen. In contrast, carbon dioxide leads to a reduction in dilution depth of approximately 60 µm. The HAZ depth remains similar for argon and helium, while nitrogen increases it by around 50 µm. Using carbon dioxide, the HAZ depth decreases by approximately 40 µm.

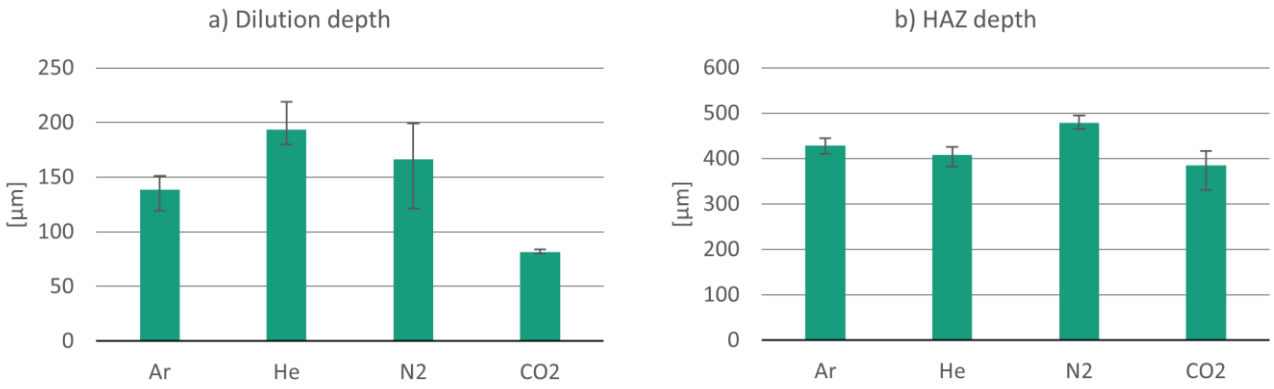

Fig. 5. (a) Depth of dilution zone and (b) depth of HAZ for the built-up volumes for different process gases

4.3. Influence of the investigated process gases on the microhardness of built-up volumes

An overview of the average hardness values for the built-up volumes depending on the process gases for the used powder material is shown in Figure 7.

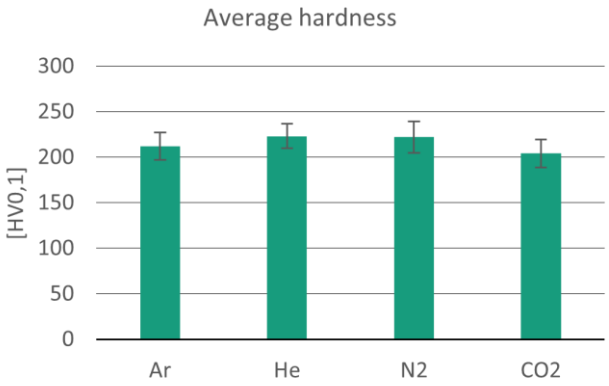

Fig. 7. Average hardness values for the built-up volumes for different process gases

Based on the averaged hardness values, no significant influence of the process gases on the microhardness of the deposited 316L volumes is initially observed. In general, higher hardness values are measured in the lower layers, which may be attributed to tempering effects and hardening mechanisms induced by energy input and heat conduction, or caused by higher cooling rate in the beginning of the process.

4.4. Analysis of surface temperatures of single tracks

Figure 8 shows the maximum process temperature for the single tracks depending on the employed process gases for the investigated powder material.

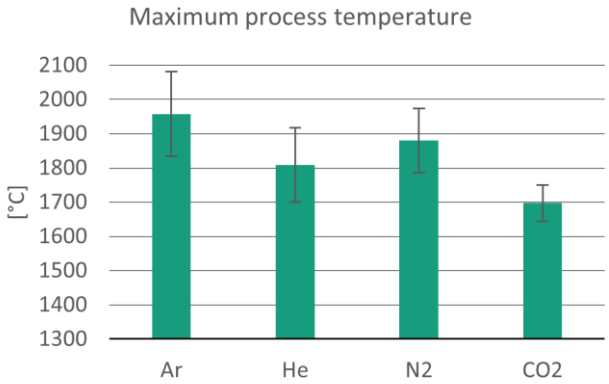

Fig. 8. Maximum process temperature for the single tracks for different process gases

When using argon as the process gas, the maximum process temperature reaches approximately 1956 °C. In comparison, it decreases by around 250 °C when using carbon dioxide, and by about 150 °C with helium. The causes of these differences in maximum temperatures between the various process gases could not be conclusively determined within the scope of this study and require further investigation.

5. Conclusion

This study analyzes the influence of the process gases argon, helium, nitrogen, and carbon dioxide on geometric characteristics of single tracks, process temperature and microhardness in laser metal deposition (LMD) using the powder material 316L. The interactions between the selected process gases and the powder material were evaluated based on single tracks and built-up volumes. The experimental results allow for a comparative assessment of the deposited material, microhardness, and maximum process temperature as a function of the process gas used:

1. For the examined powder material, no significant influence on the deposited material was observed when using argon, helium, or nitrogen as process gases. In contrast, when carbon dioxide was used, an increase in track width and a decrease in track height and wetting angle were detected. The surface characteristics of the single tracks remained largely unaffected by the choice of process gas.

2. A reduction in the dilution zone depth was observed for single tracks produced under carbon dioxide gas. In the built-up volumes, fewer powder adhesions and a smoother outer contour were identified under the same gas.

3. Microhardness measurements revealed no significant differences in hardness values between the investigated process gases for the built-up volumes of the examined powder material.

4. Compared to argon, the maximum process temperature is significantly reduced with carbon dioxide, moderately reduced with helium, and remains largely unchanged with nitrogen.

Based on the experimental results, it can be concluded that helium and nitrogen do not show a significant influence on the evaluated parameters compared to argon for the powder material 316L, and can therefore be considered suitable with respect to the investigated properties, i.e. microhardness and process temperature. In contrast, carbon dioxide as a process gas leads to distinctly different outcomes for the same material. From an economic perspective, the use of more cost-effective gases such as nitrogen or carbon dioxide offers the potential to reduce overall process costs, provided that the required material properties are maintained. For future studies, the mechanical properties of the built-up volumes should be further characterized as a function of the process gas. In future studies, potential influences on chemical composition and oxidation behavior should also be taken into account to ensure a comprehensive assessment of alternative process gases. Additionally, high-speed imaging could enable a more detailed analysis of melt pool dynamics under different shielding gas atmospheres. To deepen the understanding of process gas effects, further experimental campaigns using alternative powder materials and varying gas mixtures are recommended. Moreover, a detailed microstructural analysis of the deposited material in relation to the applied process gases should be conducted.

References

Ahn, J.; He, E.; Chen, L.; Dear, J.; Davies, C. (2017): The effect of Ar and He shielding gas on fibre laser weld shape and microstructure in AA 2024-T3. In: *Journal of Manufacturing Processes* 29, S. 62–73.

Auer, F. (2005): Methode zur Simulation des Laserstrahlschweißens unter Berücksichtigung der Ergebnisse vorangegangener Umformsimulationen. Zugl.: München, Techn. Univ., Diss., 2004. München: Utz (Forschungsberichte iwb / Institut für Werkzeugmaschinen und Betriebswissenschaften der Technischen Universität München, 192).

Bliedtner, J.; Müller, H.; Barz, A. (2013): Lasermaterialbearbeitung. München: Carl Hanser Verlag.

Candel-Ruiz, A.; Kaufmann, S.; Müllerschön, O. (2015): Strategies for high deposition rate additive manufacturing by Laser Metal Deposition. In: *Lasers in Manufacturing*.

Czerner, S. (2005): Schmelzbaddynamik beim Laserstrahl-Wärmeleitungsschweißen von Eisenwerkstoffen; Dissertation, Hannover 2005. Dissertation. Universität Hannover, Hannover.

Dobbelstein, H.; Gurevich, E. L.; George, E. P.; Ostendorf, A.; Laplanche, G. (2019): Laser metal deposition of compositionally graded TiZrNbTa refractory high-entropy alloys using elemental powder blends. In: *Additive Manufacturing* 25, S. 252–262. DOI: 10.1016/j.addma.2018.10.042.

Elmer, J. W.; Vaja, J.; Pong, R.; Gooch, T. H.; Barth, H. D. (2014): The Effect of Ar and N2 Shielding Gas on Laser Weld Porosity in Steel, Stainless Steel, and Nickel. In: *The Welding Journal*.

Härtl, J.; Zäh, M. (2002): Angepaßte Prozessgase für das Schweißen mit Hochleistungsdiodenlasern. In: *Stahl* (3), S. 66–68.

Kaljevic, A.; Demir, A. G. (2022): Influence of shielding gas flow on the µLMWD of biodegradable Mg alloy and permanent stainless steel for additive manufacturing of biomedical implants. In: *Int J Adv Manuf Technol* (119), S. 4877–4891.

Leimser, M. (2008): Strömungsinduzierte Einflüsse auf die Nahteigenschaften beim Laserstrahlschweißen von Aluminiumwerkstoffen. Dissertation, Stuttgart.

Linde Gas (2025). URL: https://www.linde-gas.de/shop/de/de-ig/home. Abrufdatum: 03.02.2025.

Ruiz, J. E.; Cortina, M.; Arrizubieta, J. I.; Lamikiz, A. (2018): Study of the Influence of Shielding Gases on Laser Metal Deposition of Inconel 718 Superalloy. In: Materials (2018) 11,. In: *Materials* (11).

Schulze G. (2010): Die Metallurgie des Schweißens. 4. Auflage: Springer Verlag.

Wank, A.; Schmengler, A.; Hitzek, A.; Kroemmer, W.; Runzka, M.; Merten, B. (2018): Influence of Process Gas Composition on Laser Cladding Process Characteristics. In: *Proceedings from the International Thermal Spray Conference*, S. 436–442.

Witzel, Johannes (2014): Qualifizierung des Laserstrahl-Auftragschweißens zur generativen Fertigung von Luftfahrtkomponenten.

Zhang, J.; Wang, H.; Cao, Y.; Su, B.; Hua, G.; Shi, T.; Shi, J. (2023): Effect of oxygen content in local shielding atmosphere on cladding quality of Ti6Al4V during annular laser metal deposition. In: *Int J Adv Manuf Technol* (128), S. 925–935.

Zhao, Kai; Chen, Mingzhi; Wang, Zhandong; Li, Rui; Jia, Zhiyuan; Lan, Huifang; Sun, Guifang (2024): Investigation of thermal and fluid dynamics behaviors of melt pool during laser direct metal deposition on inclined substrates. In: *Materials Today Communications* 41, S. 1–16. DOI: 10.1016/j.mtcomm.2024.110953.